# Spin-decoupled Multichannel Metasurface Performs the Wavevector and Frequency Multiplexing

**Keywords:** Multiplexed metasurface; spin decoupling; dual mode; wavefront control; dynamic and geometric phase

## Abstract

Achieving kaleidoscopic wavefront controls or versatile distinct functions with a thin flat plate are pivotal for increasing data capacity yet still challenging in integrated optics. Anisotropic metasurface provides an efficient recipe primarily for arbitrary linear polarization, but is less efficient for multiple functionalities at arbitrary spin states, which significantly restricts many promising applications. Here, we report a strategy to design and realize spin-decoupled high-capacity multifunctional metasurface by multiplexing the frequency and wavevector degree of freedom (DoF) of electromagnetic waves. By integrating both geometric and dynamic phases in a split ring resonators (SRRs) and crossbars in a chessboard super meta-atoms, the inherent limitation of spin-flipped Pancharatnam-Berry profiles can be completely decoupled between two spin states. Such released extraordinary DoF unprecedentedly increases the capability to yield kaleidoscopic wavefronts control. To verify the significance, two proof-of-concept metadevices that are nearly impossible in conventional metasurface have been experimentally demonstrated with the 4-port wavefront manipulations, exhibiting the spin-, frequency- and wavevector- dependent anomalous reflections, lensing, orbital angular momentum generation, wavevector-multiplexed vortices scattering, along with two-dimensional holograms, etc. Both numerical and experimental results illustrate quad distinct functionalities with up to ten channels and near 100% efficiency, thanks to the totally suppressed crosstalk among different operation modes, angular wavevectors and spins. Our finding in triple-DoF multiplexing is expected to trigger great interest in electromagnetic/optical integration with boosted information capacity and emerging DoFs.

## 1. Introduction

Performing independent multitasked wavefront control through a superthin plate is particulally promising in integration optics, and radar applications. Metasurface, in that sense, has especially intrigued the renewed interest since it affords great potentials to meet the increasing demands of high-speed and high-capacity electromagnetic (EM) devices in a flat-profile fashion. For example, the anisotropic metasurface, composed of the arrays of subwavelength meta-atoms with asymmetric structural anisotropy along two principle axes, has been proposed and demonstrated for polarization multiplexing on arbitrary two orthogonal states/spins of linearly-polarized (LP)/circularly-polarized (CP) waves (1)-(12). Instead, the vesatile functionalities could also achieved by exploiting the wavelength/frequency multiplexing that involves various multi-mode resonators, each operating individually at well separate frequencies (13)-(19). The other remarkable avenue to increase the information delivery channels in metasurface is the spatial multiplexing, which are only recently showcased in a spatially interleave closely-packed structures in several sectors of a common layer or multilayer (20)-(23). Last but not the least, the spatial angular spectrum multiplexing is another unique technique for kaleidoscopic wavefronts, which encodes versatile phase patterns on various diffraction orders (24),(25) and incidence angles (26)-(28).

Unfortunately, the common feature of above-mentioned approaches is that only single degree of freedom such as the polarization, wavelength, spatial modulation or angluarly asymmetric response was utilized, which could limit the information capacity for EM metasurface. Besides, most above strategies work primarily for arbitrary two LP waves and, as a result, the unavoidable speckle noise induced by the polarization crosstalk (7) would reduce data capacity in terms of Shannon entropy. Moreover, the emergence of compound multiplexing by mixing two or more aforementioned DoFs as information channels, more relevant to be called dual/multi-information metadevices, are still elusive and in infancy (29)-(31). In complementary to LP multitasking, spin multiplexing typically suffered inversed images or converged/diverged focusing due to locked spin-flipped phase patterns (2), (12). Moreover, the data capacity and functionalities are extremely limited since only spin was involved (12), (23), which therein may hinder the potentials in practical applications. Fortunately, emerging avenue

to decouple/unlock two spins (32)-(34) is proposed by combining both geometric and dynamic phase, which affords a powerful recipe for real spin multiplexing.

In light of the above, here, we report the concept of triple-information (spin, frequency and wavevector) multitasked metaplexer, aiming to circumvent the issue of limited system capacity. By combining unlocked dual-spin multiplexing and crosstalk-free dual-mode multiplexing, quad-port versatile independent functionalities ($F_1$, $F_2$, $F_3$ and $F_4$) that generally requires different arbitrary phase modulations ($\varphi_1$, $\varphi_2$, $\varphi_3$ and $\varphi_4$) can be engineered at dual frequencies of left-handed/spin-up (LCP/$\sigma_+$) and right-handed/spin-down (RCP/$\sigma_-$) CP waves, see Fig. 1. In fact, a maximum of $m\times n$ channels (ports) would be achieved for spin and frequency multiplexing, with $m$ and $n$ being the eigen-channels owned by each information. Furthermore, if we continue to impose $k$-kind wavevectors to each of $m\times n$ ports, a full of $m\times n\times k$ information channels would be facilitated. Thereby, this product term reveals an explosive growth of data capacity, which could even lead to full-space angular-responsible information delivery. Here, we show that such elusive scheme could be realized by hybridizing a crossbar and dual-gap split ring resonators (SRRs) in a composite meta-atom with negligible crosstalk at low and upper frequencies of $f_1$ and $f_2$ (see the inset of Fig. 1). Moreover, the high efficiency and better image quality are guaranteed by suppressing both angular and spin crosstalk. Our strategy opens up an alternative avenue for high-efficiency devices with unprecedented data capacity.

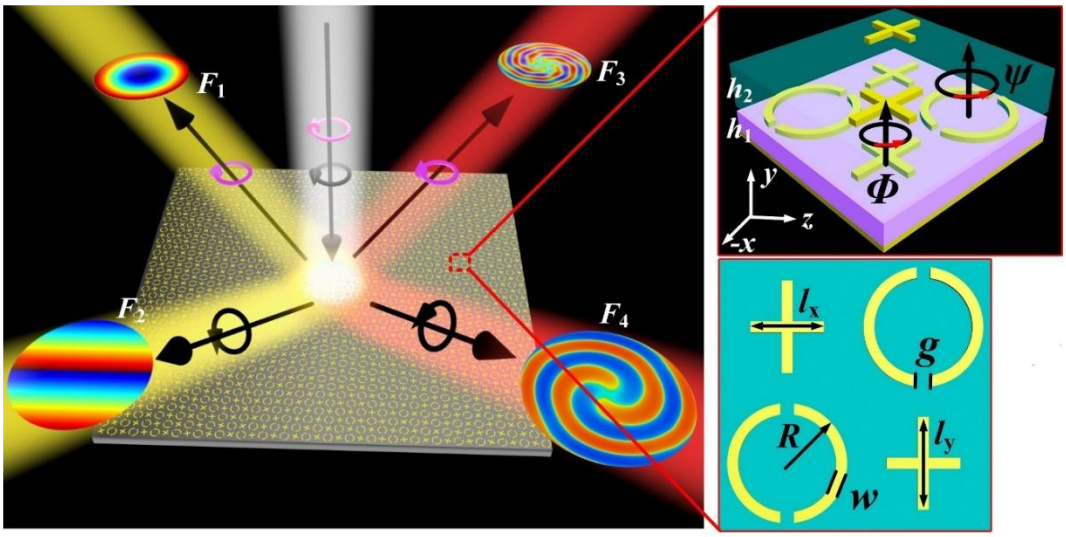


**Fig. 1 Schematic illustration of the proposed quad-port metaplexer using proposed mode- and spin-decoupled meta-atom.** The wavevector (angular) multiplexing at angle of $\phi_i$ and

$\theta_i$ on partial or full of quad channels is not shown for brevity of the figure. The function $F_1$ is achieved at the spin $\sigma_+$ and the frequency $f_1$, denoted as the eigenchannel ($\sigma_+$; $f_1$). Similarly, $F_2$, $F_3$ and $F_4$ exhibit the information channel ($\sigma_-$; $f_1$), ($\sigma_+$; $f_2$) ($\sigma_-$; $f_2$). The pixel period is $p_x$=$p_y$=20 mm. The widely available F4B dielectric board with $\varepsilon_r$=2.65 and loss tangent of 0.001 is utilized as the dual-layer substrates. The thickness of the top and bottom substrates is $h_1$=1 and $h_2$=2 mm, respectively. The other geometric parameters are $g$=2, $R$=4.4, and $w$=0.8 mm. The width of the crossbar is 0.8 and 1.4 mm while the length along x and y directions is $l_x$ and $l_y$, respectively. The full 360° phase cover is accomplished when $l_x$=$l_y$ varying within 4.8~6.8 mm.

## 2. Meta-atom with suppressed spin and mode crosstalk

The negligible spin and mode corsstalk are the key for spin and frequency multiplexing. By taking these aspects into consideration, the two constitutive counterparts should not share a concentric optical axis. As shown in Fig.1, the basic building block utilized for the multitasked metasurface is composed of dual-layer metallic patterns backed by a full metallic ground. Two types of meta-atoms are adopted in a composite chessboard configuration, say two digonal SRRs in bottom layer and two digonal crossbars in both top and bottom layer. The two counterparts exhibit suppressed mode corsstalk and each operates individually at an arbitrary frequency by cautiously tuning structure parameters. Here, the crossbars engineered in double layers are aimed to form Fabry–Perot resonance and thus accumulate a full 360° reflection phase cover under two LP waves at different frequencies. The spin-decoupled approach guarantees the completely suppressed spin crosstalk by involving both dynamic and geometric phases (34).

$$\boldsymbol{J}(x,y)=\begin{bmatrix} e^{i\varphi_1(x,y)} & e^{i\varphi_2(x,y)} \\ -ie^{i\varphi_1(x,y)} & ie^{i\varphi_2(x,y)} \end{bmatrix}\begin{bmatrix} 1 & 1 \\ i & -i \end{bmatrix}^{-1} = \boldsymbol{R}(-\Phi)\begin{bmatrix} e^{i\varphi_x} & 0 \\ 0 & e^{i\varphi_y} \end{bmatrix}\boldsymbol{R}(\Phi) \qquad (1).$$

Here, $\Phi$, $\varphi_x$, and $\varphi_y$ are eigenvalues of above symmetric and unitary Jones matrix and are related to the orientations (half of geometric phase) and dynamic phases under $x$ and $y$-polarized wave. They can be quantitatively achieved as a function of $\varphi_1$/$\varphi_3$ and $\varphi_2$/$\varphi_4$ by solving Eq. (1).

To easy the design but not lose generality, here we engineer the SRRs for dual spin-flipped phases ($\varphi_2$=-$\varphi_1$) at $f_1$ and the crossbar for dual spin-unlocked phases ($\varphi_3$ and $\varphi_4$) at $f_2$. Therein, quad structured wavefronts can be arbitrarily engineered with two similar functions at $f_1$ and

two independent ones at $f_2$ by flipping two spins of the excitation. As a consequence, only geometric phase is necessary for $F_1$ and $F_2$ by rotating the SRRs with different $\Psi$, whereas both geometric and dynamic phases are required to decouple $F_3$ and $F_4$ by simutaneously altering both the structural parameters and orientations $\Phi$. Note that the phase profiles at $f_1$ also can be completely decoupled for $\sigma_+$ and $\sigma_-$ state by additionaly varying the gap of SRRs, which is not within the scope of this work. Interestly, the polarization crosstalk (34) between two orthogonal LP waves could signinficantly deteriorate the efficiency and fidelity of $F_3$ and $F_4$ at $f_2$, while our adopted narrow bar instead of wide patch would nearly perfectly suppress the aforementioned LP crosstalk.

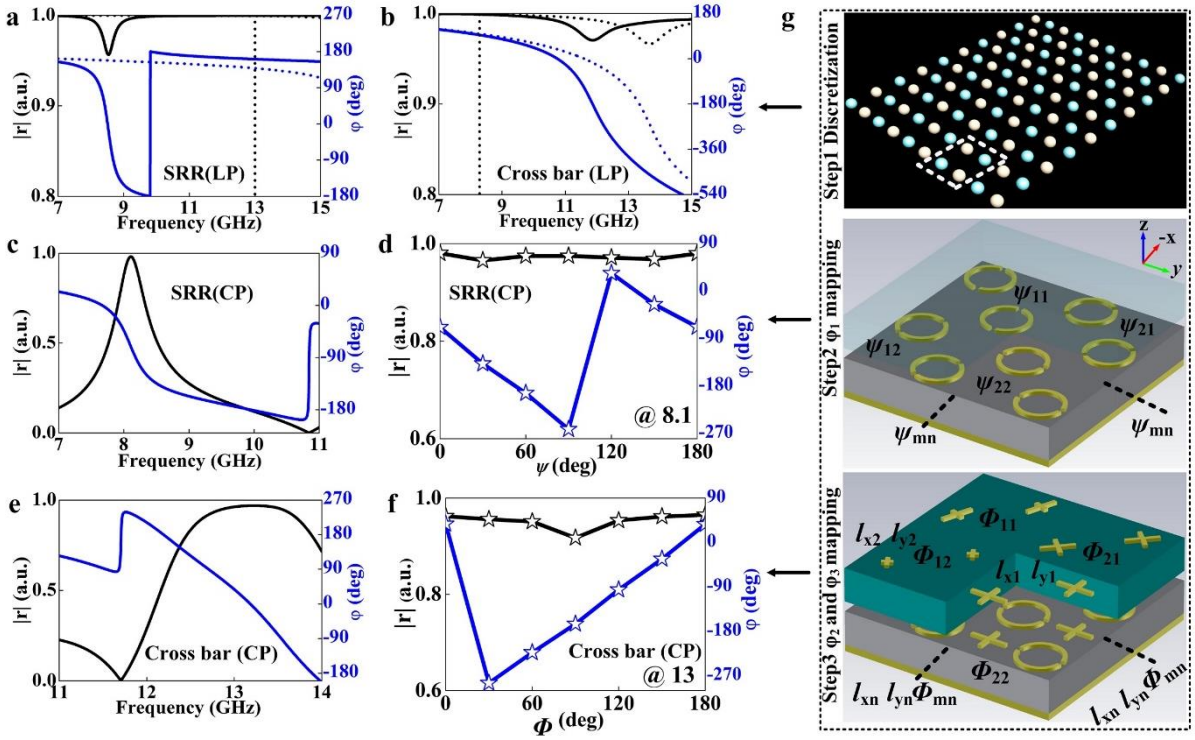


**Fig. 2 (a-f) Characterization of the basic meta-atom and (g) the three-step design process.** Reflection magnitude and phase response of the individual (a) SRRs and (b) crossbar under x- and y-polarized LP wave. (c) Co-CP reflection magnitude and phase response of the composite meta-atom at (c, d) low and upper (e, f) bands under spin state of $\sigma_+$ or $\sigma_-$ varying as (c, e) frequency and (d, f) orientations. Here, the two sub-meta-atoms are represented by orange and blue in (g).

To characterize the EM response and performance, the subwavelength meta-atom and all resulting metaplexers were evaluated by performing full-wave finite-difference time-domain (FDTD) simulations in the commercial packet of CST Microwave Studio, see experimental

section for details. As shown in Fig. 2(a) and 2(b), both the SRRs and crossbar exhibit obvious anisotropy around $f_1$=8.1 and $f_2$=13 GHz, where shifted spectrum response is clearly inspected under two orthogonal LP waves. The shallow dip facilitates near-unity reflection with magnitude larger than 0.96 across the entire observed band, whereas the shifted phase response enables the 180° out-of-phase difference between $\varphi_y$ and $\varphi_x$. Most importantly, both SRRs and crossbar manifest negligible phase tolerance at high and low frequency, respectively, implying a completely suppressed mode crosstalk between the two structures which thus can be individually designed. Such a merit is the key for the frequency multiplexing. Under the condition of $|r_{yy}|\approx|r_{xx}|$ and $|\varphi_y-\varphi_x|\approx180^o$ at $f_1$ and $f_2$, near 100% efficiency can be engineered for co-CP reflection with almost suppressed cross component, as shown in Fig. 2(c) and 2(e). The geometric phases at $f_1$ and $f_2$ can be individually engineered by rotating SRRs and crossbar along its local optical axis with $\Psi$ and $\Phi$ ranging from 0° to 180°. As expected in Fig. 2(d) and 2(f), very coincident linear phase response $\varphi\approx2\Psi$ ($2\Phi$) as theoretical anticipation and near-unity amplitude are clearly appreciated. Moreover, the dynamic phase of the crossbar is accomplished by altering its length of $l_x$ and $l_y$ based on $\varphi_x$-$l_x$ and $\varphi_y$-$l_y$ relation shown in Fig. S1 of Supporting Information, where a full 2π phase cover ranging from 12.5 to 13.5 GHz is fulfilled by varying $l_y$ within 4.8~6.8 mm. Such a level of full-phase bandwidth is very considerable for spin-unlocked versatile wavefront control. Similar $\varphi_x$-$l_x$ relation can be expected the same as $\varphi_y$-$l_y$ due to the four-fold rotation symmetry. The outstanding phase tolerance to $\varphi_y$ induced by the change of $l_x$ is less than 40°, indicating a negligible polarization crosstalk. Such a feature is very beneficial for spin multiplexing.

Above exotic feature of our proposed scheme can be readily utilized to develop multiplexed metadevices with high capacity and efficiency. The design process is simple and mainly involves three steps. As shown in Fig. 2(g), the first step is discretizing the metasurface with a set of pixels and cautiously designing two types of sub-meta-atoms that exhibit negligible eigen-channel crosstalk in a chessboard configuration. Since SRRs and crossbars constitute the hybrid meta-atom, the phase mapping of imposed $\varphi_1$ and $\varphi_2$ can be implemented according to the predefined functionalities ($F_1$ and $F_2$) at $f_1$ by spatially rotating $\Psi$ of each SRRs to induce the geometric phase. Finally, determine layouts ($l_x$, $l_y$ and $\Phi$) of spatially varied crossbars according to $\varphi_x$, $\varphi_y$, and $\Phi$ by mapping the phase patterns of $\varphi_3$ ($F_3$) and $\varphi_4$ ($F_4$) at $f_2$ following

Equation (1).

## 3. Wavevector multiplexing principle

Here, we will briefly introduce the fundamental principle for additional wavevector multiplexing, which is on the basis of mixing phase in a shared aperture and thereby is quite different from the grating (12), interleaved (20) and harmonic-response approach (24), (25). The synthetic wavevector and mixing phase can be arbitrarily engineered according to predefined composite functions. Here, to facilitate versatile wavevectors, multibeam scatterings carrying different topological charges (modes) of orbital angular momentum (OAM) are explored as an example. The synthetic wavevector $\vec{k}_\rho$ and required phase pattern $\varphi$(x, y) can be formulated as

$$\exp(i\vec{k}_\rho\vec{\rho})=\exp(i\varphi(x,y)) = m_i[\sum_{i=1}^{k}\exp(-il_i\phi)+\sum_{i=1}^{k}\exp(ik_{xi}x)+\sum_{i=1}^{k}\exp(ik_{yi}y)] \qquad (2).$$

Here, $\vec{\rho}=xx+yy$, $k$ is the required beam number, $m_i$ and $l_i$ are tailored intensity and the topological charge of the $i^{th}$ spatial beam, $k_{xi}=k_0*\cos(\phi_i)\sin(\theta_i)$ and $k_{yi}=k_0*\sin(\phi_i)\sin(\theta_i)$ are decomposed wavevectors of the $i^{th}$ beam along $x$ and $y$ directions, $\phi_i$ and $\theta_i$ are azimuth and elevation angle of each beam. Equation (2) reveals a boosted versatility of our approach, which is co-determined by the scattering intensity, OAM modes, beam numbers and beam directions. Moreover, the unique merit consists in that the $m_i$, $l_i$, $k$, $\phi_i$ and $\theta_i$ can be arbitrarily controlled. These extraordinary DoF and increased capacity are extremely difficult to be realized through available approaches. It is pivotal to discuss the angular channel capacity limit, i.e., the upper limit of $k$. The signal-to-noise ratio (SNR) intensity per channel, which is related to the angular crosstalk, determines the $k$ and has been demonstrated deceasing as $1/k^2$ (20). Thereby, the breakthrough of our mixing approach for wavevector multiplexing lies in the extremely boosted $k$ determined by the SNR, particularly relative to the grating approach (12) whose beam is limited to two.

## 4. Triple-information multitasked metaplexer I

As the proof-of-concept demonstration, we first design a metaplexer by performing partial wavevector multiplexing with inversed reflection angles on $F_1$ and $F_2$ channel under $\sigma_+$ and $\sigma_-$ state of $f_1$=8.1 GHz, while manifesting light focusing capability ($F_3$) and specular spiral-beam generation ($F_4$) under identical spin states of $f_2$=13 GHz. Here, quad asymmetric scattering beams of different OAM modes are adopted for wavevector multiplexing with predesigned $m_i$=1, $l_i$=0, 1, 2 and 3, $k$=4, and ($\phi_i$; $\theta_i$)=(0°, 90°, 180°, 270°; 15°). The target phases of $\varphi_1$~$\varphi_4$ can be observed from Fig. 3(a) and Fig. S2(a), where a composite, parabolic and spiral phase profile are clearly observed. Following aforementioned theoretical strategy, $\varphi_x$, $\varphi_y$ and $\Phi$ can be derived to decouple $F_3$ and $F_4$ with unlocked $\varphi_3$ and $\varphi_4$ at two helicity. For this purpose, a total of 360° phase cover and near 100% efficiency should be fulfilled when $l_y$ varies within 4.8~6.8 mm, see Fig. S1 in Supporting Information. The final hybrid metaplexer can be mapped out according to $\varphi_1$, $\varphi_x$, $\varphi_y$ and $\Phi$, as shown in Fig. 3(a). For experimental verification, all proof-of-concept samples shown in Fig. 3(b) and Fig. 4(b) were fabricated with near- and far-field results measured in a microwave anechoic chamber, see experimental section.

As shown in Fig. 3 (c), four distinct wavefronts are clearly obereved at $\sigma_+$/$\sigma_-$ states of two well seperated frequencies. The switch among dot- and donut-shaped scattering patterns with gradually enlarged pattern aperture indicates sequential vortices of OAM modes of $l$=0, 1, 2, and 3 for $F_1$ and $F_2$. Such a declaration finds direct support from the measured near-field Re($E_{\sigma+/\sigma-}$) distributions shown in Fig. 3 (d), where four localized patterns with different spiral arms of 0, 1, 2 and 3 are clearly observed. The well angular-resolved multibeams exhibit negligible noise and thus enable to provide high information capacity. Such multiple vortices ($F_1$/$F_2$) can be transformed into unique one ($F_4$) by switching operaion mode from $f_1$ to $f_2$. Most importantly, the almost completely suppresed specular mode in $F_1$/$F_2$ and very low sidelobe in $F_4$ imply a near 100% efficiency which benefits considerably from the extremely low angular crosstalk. Such a level of efficiency is in good consistency with that of pure anomalous reflection at $F_1$/$F_2$ channel shown in Fig. S3 of Supporting Information, indicating the reasonablity of mixing-phase approach. The experimental donut-shaped $|E_{\sigma+/\sigma-}|$ intensity with sequentially enlarged ring spots coincides well with the increased FDTD calculated amplitude-null (optical singularity) scattering patterns. This can be further evidenced from the well-agreed

far-field crosssection patterns between FDTD simulations and measurements shown in Fig. S4, where all beams are nearly directed toward ($\phi_i$; $\theta$)=(0$^o$, 90$^o$, 180$^o$, 270$^o$; 15$^o$). Moreover, the peak intensity decreases as the OAM mode increases. The physics lies in that enlarged ring spot consumes more power and the energy conservation compels the peak to fall.

The measured $E_{\sigma+/\sigma-}$ intensity for $F_3$ again agrees reasonably with the FDTD calculated ones, indicating fine light focusing with concave and convex wavefronts sandwiched by a clear focusing spot near $F$=115 mm ($F$=126 mm in theory) before the metaplexer. The reversed wavefronts evolved along opposite longitudinal axis resembles two waves emitting from an emerging source (spot). The full width at half maximum (FWHM) of the focusing spot is evaluated about ~ 17 mm at focal plane of $z$=118 mm. which is very close to the theoretical limit of 16.4 mm determined by aperture size and focal length. The minor deviations between simulations and measurements can be ascribed to slight misalignment of source/receiver antennas and nonideal plane wave excitations. To sum up, all quantitative results reveal four predefined functionalities of ten channels under spin-up/down waves, i.e., two wavevector-multiplexed quad-beam vortices scatterings with reversed direction angles, and fine light focusing/specular OAM generation.

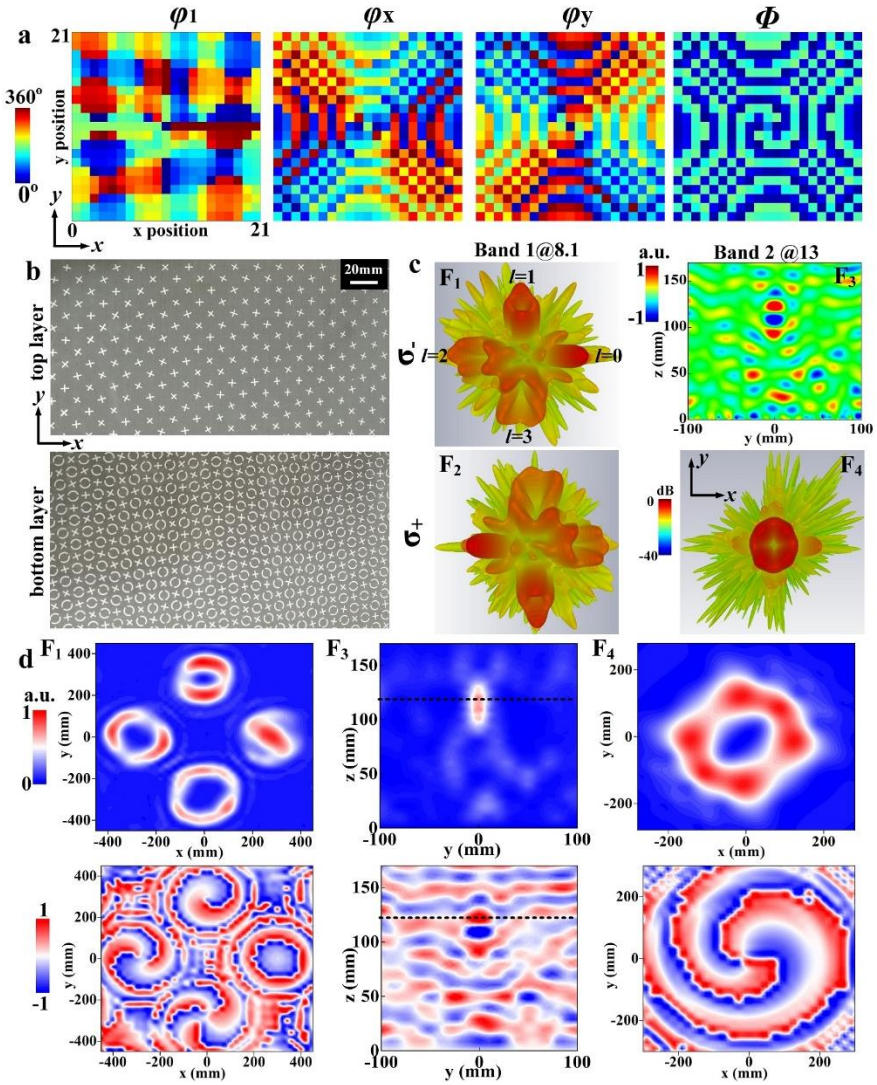


**Fig. 3** Characterization of the triple-information multitasked metaplexer I with two wavevector-multiplexed quad-beam vortices scatterings in reversed angles and different OAM modes, light focusing and specular spiral beam generation. The metaplexer contains 21*21 hybrid pixels and accommodates a square area of 420*420 mm$^2$. For $F_1$ and $F_2$, the oblique OAM modes are orderly as $l$=0, 1, 2, and 3, whereas the direction angles are predesigned as ($\phi_i$; $\theta_i$)=(0°, 90°, 180°, 270°; 15°). For $F_3$, the focal length is predesigned as $F$=420*0.3=126 mm, whereas for $F_4$ the specular OAM mode is $l$=2. (a) Theoretically synthetic composite phase patterns for $F_1$, $F_2$, and derived dynamic and geometric phases of $\varphi_x$, $\varphi_y$, $\Phi$ to decouple $F_3$ and $F_4$ into two indepedent spin channels. (b) A magnified view of finally fabricated metaplexer sample with the top and bottom layer. (c) FDTD calculated far-field steered and specular vortex scatterings patterns ($F_1$, $F_2$ and $F_4$), and Re($E_{\sigma+/\sigma-}$) field distributions on yz plane ($F_3$) under σ+ and σ- waves of $f_1$ and $f_2$. (d) Experimentally measured near-field intensity $|E_{\sigma+/\sigma-}|$ and Re($E_{\sigma+/\sigma-}$) on xy

(z=4 m for $F_1$ and z=0.5 m for $F_4$) and yz (x=0 mm) plane by scanning an area of 0.9×0.9 $m^2$, 0.2×0.18 $m^2$ and 0.6×0.6 $m^2$ in steps of 8 mm to illustrate kaleidoscopic wavefronts of $F_1$, $F_3$ and $F_4$. Here, measured results for similar functionality of $F_2$ is not given for brevity of contents. The efficiency was defined as the ratio of the sum of the power associated with all anomalously steered OAM beams to the totally reflected power ($\int_0^{2\pi}\int_{-\pi/2}^{\pi/2} P(\theta,\phi)d\theta d\phi$) of a PEC plate of the same size.

## 5. Triple-information multitasked metaplexer II

To make a step forward, here we further demonstrate the possible applications of our strategy by characterizing a metaplexer with multitasked EM computer generated holography (CGH). The significance of utilizing hybrid strategy for multiplexing holograms under two independent helicity states lies in the avoidable sophisiticated optimization process (23). Instead, it is deterministic when two holographic phase patterns is given. Moreover, the data capacity is significantly enlarged as twice of previous report. To suppress undersirable parasitic diffractions in terms of finite-size effect, we utlize more pixels for better image quality. As shown in Fig. 4(a) and Fig. S6 in Supporting Information, a total of 30*30 hybrid pixels that accommodate an area of 600*600 $mm^2$ are utilized to construct the sophisticated metaplexer imprinted with abundant wavefronts and holograms. Here, we encode multiple vortices of symmetric and asymmetric beams along two principal axes for wavevector-multiplexed $F_1$/$F_2$, but impose wavefronts of reconstructed image of letter 'A' and 'B' for $F_3$ and $F_4$ under $\sigma_+$/$\sigma_-$ spin state, respectively. Quad beams with topological charges of $l$=0, 1, 2 and 1, and sidelobes less than -40 dB are precisely engineered toward ($\phi_i$; $\theta$)=($0^o$, $90^o$, $180^o$, $270^o$; $15^o$). The phase profiles for hologram images of letters 'A' and 'B' are designed in a way analogous to that of classical Gerchberg-Saxton (GS) algorithm, except for replacement of the fast Fourier transform by the first Rayleigh-Sommerfeld diffraction integral, given by

$$U_2(x_2,y_2)=\frac{z}{j\lambda}\iint_{\Sigma}\frac{U_1(x_1,y_1)\exp(jkr_{12})}{r_{12}^2}dx_1dy_1 \quad (3).$$

Here, $U_1(x_1, y_1)$ and $U_2(x_2, y_2)$ are field distributions on the hologram and target plane, respectively, $z$ and $r_{12}$ are the projection and distance between arbitrary two points of the two

planes. Σ is the hologram domain, $\lambda$ is the wavelength and $k$ is the wave number in free space. The rigorous integral above can be evaluated by a discrete summation and detailed phase-retrieving process can be referred to Fig. S5 in Supporting Information.

The calculated phase distribution for quad vortices and the eventually optimized phases for dual images of 'A' and 'B' are shown in the top row of Fig. 4(a), whereas the decoupled phase profiles for $F_3$ and $F_4$ can be appreciated from the bottom row. By following the three-step design process, the final metaplexer is fabricated using multilayer printed circuit board fabrication process, see Fig. 4(b) for magnified view. As expected in Fig. 4(c) and 4(d), two asymmetric and two symmetric vortices are clearly inspected along $x$ and $y$ axis, respectively. The dot- and donut-shaped patterns of different sizes identify different OAM modes of $l$=0, 1, 2 and 1 in anticlockwise. The flipped phase from $\sigma_+$ to $\sigma_-$ state only reverses the spatial direction of the vortices. Again, the peak intensity lows down as the OAM mode increases due to enlarged ring spots. Versatile OAM modes can be directly evidenced from the number of measured spiral arms shown in left panel of Fig. 4(e). The channel mixing of different phases for $F_1$~$F_4$ does not pose much penalty on the fundamental behavior and efficiency of kaleidoscopic vortices scattering, except for the shrunk beam size of metaplexer II due to the enlarged aperture size relative to metaplexer I. The negligible specular backward scattering reveals near-unity efficiency. In sharp contrast, two distinct images of letters 'A' and 'B' with remarkable image quality are clearly observed from right panel of Fig. 4(e) by flipping the spin. Moreover, the reconstructed hologram image sacrifices slighly as the observation point and operation frequency deviate from $z_0$=0.52 m and $f_2$=13 GHz, see Fig. S7 and S8 in Supporting Information for results at off-$f_2$ frequencies. Nevertheless, it does not poes much penlty within $z_0$±0.06 m and $f_2$±0.5 GHz, indicating a good robustness of our metahologram. The SNR, defined as the scale of the peak image intensity to the background noise, is evaluated near 8.1 dB for holograms at 0.52 m and deterioriates slightly to 7 dB at other observed positions and frequencies. Such a level of SNR is quite considerable for avaiable limited pixels relative to reprogrammable hologram (35), and more pixels would facilidate better SNR and image qualities. All the results above clearly illustrate kaleidoscopic wavefronts at four information channels, further verifying our concept and design.

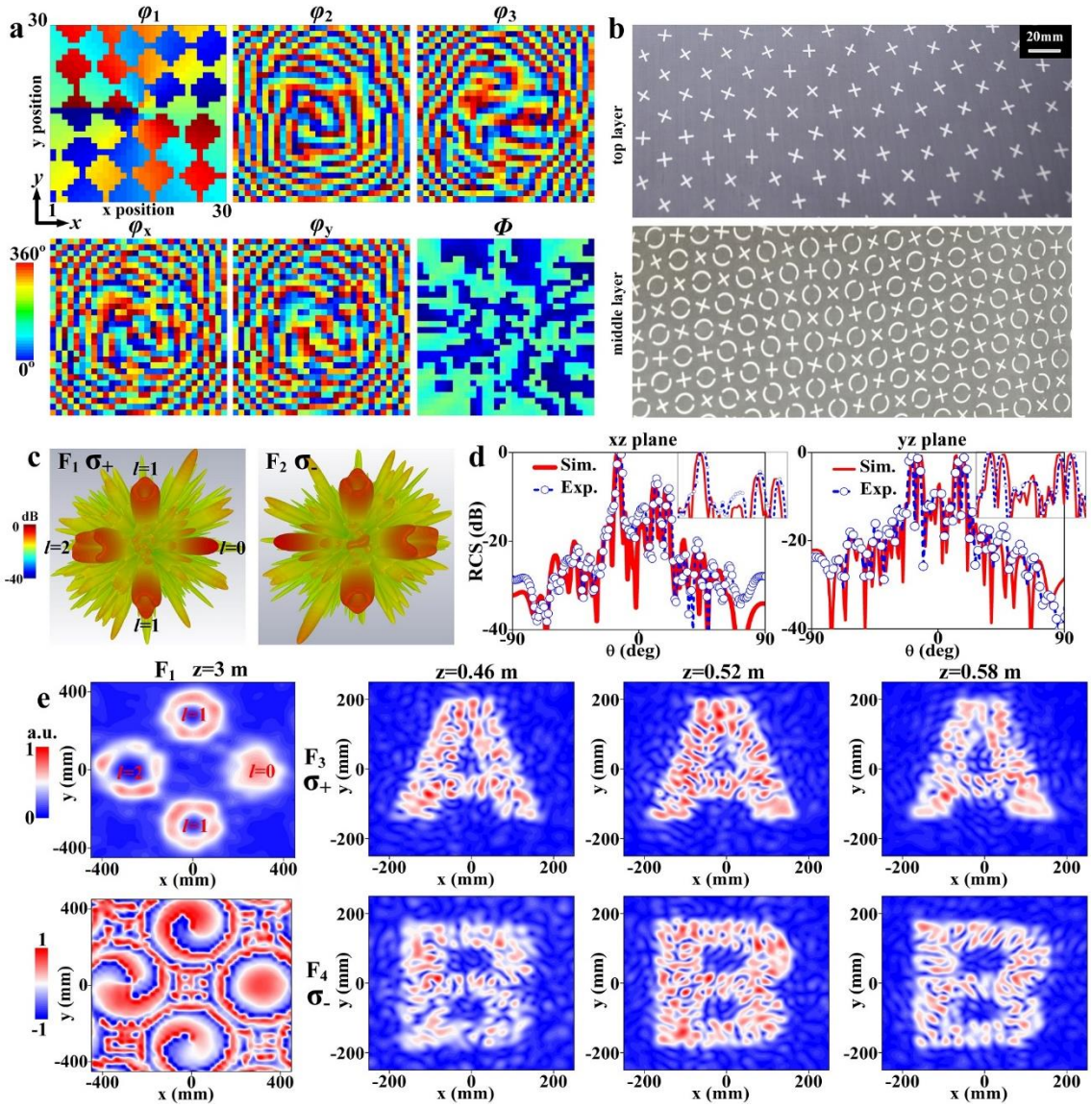


**Fig. 4** Characterization of the triple-information multitasked metaplexer II with wavefronts of two reversed wavevector-multiplexed quad-beam vortices scattering and two distinct hologram images. (a) Synthetic phase (top row) for quad vortices ($F_1$/$F_2$) and optimized phases for dual hologram images of 'A' and 'B' ($F_3$ and $F_4$) based on modified GS algorithm, and the derived dynamic and geometric phases (bottom row) of $\varphi_x$, $\varphi_y$, $\Phi$ to decouple $F_3$ and $F_4$. (b) A magnified view of the finally fabricated metaplexer with top and bottom layer. (c) FDTD calculated 3D far-field patterns and (d) experimentally measured cross section patterns on xz and yz planes for $F_1$/$F_2$. (e) Measured near-field Re($E_{\sigma+/\sigma-}$) and $|E_{\sigma+/\sigma-}|$ distributions by scanning an area of 0.9×0.9 $m^2$ and 0.5×0.5 $m^2$ in steps of 8 mm to illustrate kaleidoscopic vortices (left panel) and hologram images of 'A' and 'B' (right panel) for $F_1$, $F_3$ and $F_4$.

## 6. Conclusion

To sum up, we have proposed and demonstrated the concept of frequency-and-wavevector multiplexing under the spin-decoupled framework for structured wavefronts. In this regard, a composite meta-atom of crossbar and dual-gap split ring resonators (SRRs) is devised with negligible mode and spin crosstalk. The reasonability of the triple-DoF multiplexing has been verified by two well-designed kaleidoscopic metaplexers operated at microwave frequencies. Consistent numerical and experimental results qualify our proposed hybrid strategy a solid platform to realize well spin/mode/angular resolved systems with high information capacity and efficiency. Albeit an operation in reflection scheme, our finding can be readily extended to transmission geometry, and other high-efficiency achromatic devices at multiple frequencies due to the unlocked arbitary phase profiles.

## 7. Experimental section

**Numerical characterizations.** All numerical designs and characterizations are performed through FDTD simulations in CST Microwave Studio package. Specifically, in calculations of the reflection amplitudes/phases of the metasurface, we only studied the basic composite meta-atom with periodic boundary conditions imposed at its four bounds, and with a Floquet port placed at a distance 15 mm away from the meta-atom plane. In near-field and far-field characterizations, the metaplexer composed of spatially varied meta-atoms, is investigated with open boundary applied at its four bounds of plane. In all scenarios, the metaplexers/meta-atoms are illuminated by a normally incident plane wave under LP, spin-up or spin-down CP stimulation.

**Sample fabrication and microwave experiments.** The dual-layer metallic patterns of each metaplexer were fabricated individually on two dielectric boards using printed circuit board technique. They were first aligned with each other through several embedded vias, then assembled together through adhesives, and finally reinforced through a hot press. To avoid any possible interference from the environment, all far-field (FF) and near-field (NF) microwave experiments are performed in an anechoic chamber, see the experimental setup shown in Fig. S9. In NF measurements, the metaplexer sample was excited by a CP horn with an axial ratio of less than 3.5 dB, and a voltage-standing-wave ratio of less than 2.5 in 8~18 GHz. A 15 mm-long monopole antenna, functioning as the receiver, was placed between the sample and CP

horn which were fixed with a distance of 1.8 m, and was linked to a N5230C Agilent vector network analyzer to record the static EM signals. The monopole was fixed to a 2D electronic step motor that can move automatically in a maximum area of 1.2 m × 1.2 m with a step resolution of 8 mm. By shifting the monopole orientation along *x* and *y* directions, both local $E_x$ and $E_y$ field can be obtained (with both amplitude and phase). Then the spin-up and spin-down components can be calculated as $E_{LCP} = \frac{1}{\sqrt{2}}(E_x - iE_y)$ and $E_{LCP} = \frac{1}{\sqrt{2}}(E_x + iE_y)$ by incorporating both measured information. By altering the relative position of the metaplexer and 2D monitor, we can achieve the field information in xz, yz and xy planes. In all near-field contour maps, the incident signal in free space was deducted from the total fields. In the FF RCS measurements, two CP horns are adopted as the transmitter and receiver, and are displaced 1.8 m apart from the sample. The receiving CP horn, which was aligned with the metaplexer, rotated freely to record the signal scattered within $-90^o < \theta_r < 90^o$. In the FF quad-beam pattern measurements, the metaplexer was fed by a small CP horn, and both of them were fixed on a large rigid foam which is capable of rotating freely along the foam's axial center. The CP receiver was placed 10 m away to record the far-field signals.

## Acknowledgements

This work was supported by the National Natural Science Foundation of China (61501499); Youth Talent Lifting Project of the China Association for Science and Technology (17-JCJQ-QT-003); Key Program of Natural Science Foundation of Shaanxi Province (2017KJXX-24). National Key Research and Development Program of China (2017YFA0700202).

## References

(1) Kats, M. A.; Genevet, P.; Aoust, G.; Yu, N.; Blanchard, R.; Aieta, F.; Gaburro, Z.; Capasso, F. Giant birefringence in optical antenna arrays with widely tailorable optical anisotropy. *Proc. Nat. Acad. Sci.* **2012**, 109, 12364-12368.

(2) Chen, X.; Huang, L.; Mühlenbernd, H.; Li, G.; Bai, B.; Tan, Q.; Jin, G.; Qiu, C. W.; Zhang, S.; Zentgraf, T. Dual-polarity plasmonic metalens for visible light. *Nat Commun.* **2012**, 3, 1198.

(3) Pors, A.; Albrektsen, O.; Radko, I. P.; Bozhevolnyi, S. I. Gap plasmon-based metasurfaces for total control of reflected light. *Sci. Rep.* **2013**, 3, 2155.

(4) Chen, W. T.; Yang, K. Y.; Wang, C. M.; Huang, Y. W.; Sun, G.; Chiang, I. D.; Liao, C. Y.; Hsu, W. L.; Lin, H. T.; Sun, S.; Zhou, L. High-efficiency broadband meta-hologram with polarization-controlled dual images. *Nano Lett.* **2014**, 14, 225–230.

(5) Huang, Y. W.; Chen, W. T.; Tsai, W. Y.; Wu, P. C.; Wang, C. M.; Sun, G.; Tsai, D. P. Aluminum plasmonic multicolor meta-hologram. *Nano Lett.* **2015**, 15, 3122-3127.

(6) Liu, S.; Cui, T. J.; Xu, Q.; Bao, D.; Du, L.; Wan, X.; Tang, W. X.; Ouyang, C.; Zhou, X. Y.; Yuan, H.; Ma, H. F. *Light: Sci. Appl.* **2016**, 5, e16076.

(7) Xu, H. X.; Tang, S.; Ling, X.; Luo, W.; Zhou, L. Flexible control of highly-directive emissions based on bifunctional metasurfaces with low polarization cross-talking. *Annalen der physik* **2017**, 529, 201700045.

(8) Cai, T.; Wang, G.; Tang, S.; Xu, H. X.; Duan, J.; Guo, H.; Guan, F.; Sun, S;. He, Q.; Zhou, L. High-efficiency and full-space manipulation of electromagnetic wave fronts with metasurfaces. *Phys. Rev. Appl.* **2017**, 8, 034033.

(9) Xu, H. X.; Zhang, L.; Kim, Y.; Wang, G. M.; Zhang, X. K.; Sun, Y.; Ling, X.; Liu, H.; Chen, Z.; Qiu, C. W. Wavenumber-splitting metasurfaces achieve multi-channel diffusive invisibility. *Adv. Opt. Mater.* **2018**, 6, 1800010.

(10) Z.-L. Deng, J. Deng, X. Zhuang, S. Wang, T. S., G. P. Wang, Y. Wang, J. Xu, Y. Cao, X. Wang, X. Cheng, G. Li and X. Li, Facile metagrating holograms with broadband and extreme angle tolerance, *Light: Sci. Appl.* 2018, 7:78

(11) J. Zhou, H. Qian, G. Hu, H. Luo, S. Wen, and Z. Liu, Broadband photonic spin hall meta-lens, *ACS Nano* **2018**, 121, 82-88.

(12) H.-X. Xu, G. Hu, Y. Li, L. Han, J. Zhao, Y. Sun, F. Yuan, G.-M. Wang, Z. H. Jiang, X. Ling, T. J. Cui, C.-W. Qiu, Interference-assisted kaleidoscopic meta-plexer for arbitrary spin-wavefront manipulation. *Light: Sci. Appl.* **2019**, 8: 3.

(13) Aieta, F.; Kats, M. A.; Genevet, P.; Capasso, F. Multiwavelength achromatic metasurfaces by dispersive phase compensation, *Science* **2015**, 347, 6228, 1342−1345.

(14) Montelongo, Y.; Tenorio-Pearl, J. O.; Williams, C.; Zhang, S.; Milne, W. I.; Wilkinson, T. D. Plasmonic nanoparticle scattering for color holograms. *Proc. Natl. Acad. Sci.* **2014**, 111, 12679−12683.

(15) Arbabi, E.; Arbabi, A.; Kamali, S. M.; Horie, Y.; Faraon, A. Multiwavelength polarization-insensitive lenses based on dielectric metasurfaces with meta-molecules. *Optica* **2016**, 3, 628−633.

(16) B. Wang, F. Dong, Q. T. Li, D. Yang, C. Sun, J. Chen, Z. Song, L. Xu, W. Chu, Y. F. Xiao, Q. Gong, and Y. Li, "Visible-frequency dielectric metasurfaces for multiwavelength achromatic and highly dispersive holograms," *Nano Lett.* **2016**, 16, 5235–5240.

(17) J. Ding, S. An, B. Zheng, H. Zhang, "Multiwavelength metasurfaces based on single-layer dual-wavelength meta-atoms: toward complete phase and amplitude modulations at two wavelengths", *Adv. Opt. Mater.* **2017**, 5, 1700079.

(18) Y. Zhou, I. I. Kravchenko, H. Wang, J. R. Nolen, G. Gu, and J. Valentine, Multilayer noninteracting dielectric metasurfaces for multiwavelength metaoptics, *Nano Lett.* **2018**, 18, 12, 7529-7537.

(19) Guo Dong Bai, Qian Ma, Shahid Iqbal, Lei Bao, Hong Bo Jing, Lei Zhang, Hao Tian Wu, Rui Yuan Wu, Hao Chi Zhang, Cheng Yang, and Tie Jun Cui, Multitasking shared aperture enabled with multiband digital coding metasurface, *Adv. Opt. Mater.* **2018**, 1800657.

(20) E. Maguid, I. Yulevich, D. Veksler, V. Kleiner, M. L. Brongersma, E. Hasman, "Photonic spin-controlled multifunctional shared-aperture antenna array," *Science* **2016**, 352, 1202-1205.

(21) Mei, S.; Mehmood, M. Q.; Hussain, S.; Huang, K.; Ling, X.; Siew, S. Y.; Liu, H.; Teng, J.; Danner, A.; Qiu, C. W. Flat helical nanosieves. *Adv. Funct. Mater.* **2016**, 26, 5255-5262.

(22) Mehmood, M. Q.; Mei, S.; Hussain, S.; Huang, K.; Siew, S. Y.; Zhang, L.; Zhang, T.; Ling, X.; Liu, H.; Teng,

J.; Danner, A. Visible-frequency metasurface for structuring and spatially multiplexing optical vortices. *Adv. Mater.* **2016**, 28, 2533-2539.

(23) Q. Wang, E. Plum, Q. Yang, X. Zhang, Q. Xu, Y. Xu, J. Han and W. Zhang, Reflective chiral meta-holography: multiplexing holograms for circularly polarized waves, *Light: Sci. Appl.* **2018** 7:25

(24) T. Lei, M. Zhang, Y. Li, P. Jia, G. N. Liu, X. Xu, Z. Li, C. Min, J. Lin, C. Yu, H. Niu and X. Yuan, Massive individual orbital angular momentum channels for multiplexing enabled by Dammann gratings, *Light: Sci. Appl.* 4, e257, (2015).

(25) Z.H. Jiang, L. Kang, W. Hong, and D. H. Werner, Highly efficient broadband multiplexed millimeter-wave vortices from metasurface-enabled transmit-arrays of subwavelength thickness, *Phys. Rev. Applied* 9, 064009 (2018)

(26) X. Zhang, M. Pu, Y. Guo, J. Jin, X. Li, X. Ma, J. Luo, C. Wang, and X. Luo, Colorful metahologram with independently controlled images in transmission and reflection spaces, *Adv. Funct. Mater.* **2019**, 1809145.

(27) X. Li, L. Chen, Y. Li, X. Zhang, M. Pu, Z. Zhao, X. Ma, Y. Wang, M. Hong, and X. Luo, "Multicolor 3D meta-holography by broadband plasmonic modulation," *Sci. Adv.* **2016**, 2, e1601102.

(28) S. M. Kamali, E. Arbabi, A. Arbabi, Yu Horie, M. Faraji-Dana, and A. Faraon, Angle-multiplexed metasurfaces: encoding independent wavefronts in a single metasurface under different illumination angles, *Physical Review X* **2017**, 7, 041056.

(29) L. Huang, H. Muhlenbernd, X. Li, X. Song, B. Bai, Y. Wang, et al., "Broadband Hybrid Holographic Multiplexing with Geometric Metasurfaces," *Advanced Materials* **2015**, 27, 6444-6449.

(30) Wang, Q. et al. Polarization and frequency multiplexed terahertz metaholography. *Adv. Opt. Mater.* **2017**, 5, 1700277.

(31) Lei Zhang, Rui Yuan Wu, Guo Dong Bai, Hao Tian Wu, Qian Ma, Xiao Qing Chen, and Tie Jun Cui, Transmission-reflection-integrated multifunctional coding metasurface for full-space controls of electromagnetic waves, *Adv. Funct. Mater.* **2018**, 28, 1802205.

(32) Mueller, J. P. B.; Rubin, N. A.; Devlin, R. C.; Groever, B.; Capasso, F. Metasurface polarization optics: independent phase control of arbitrary orthogonal states of polarization. *Phys. Rev. Lett.* **2017**, 118, 113901.

(33) Devlin, R. C.; Ambrosio, A.; Rubin, N. A.; Mueller, J. P. B.; Capasso, F. Arbitrary spin-to–orbital angular momentum conversion of light. *Science* **2018**, 358, 896–901.

(34) H.-X. Xu, L.Han, Y. Li, Y. Sun, J. Zhao, S. Zhang, C.-W. Qiu. Completely spin-decoupled dual-phase hybrid metasurfaces for arbitrary wavefront control. *ACS Photonics* **2019**, 6(1), 211-220.

(35) L. Li, T. J. Cui, W. Ji, S. Liu, J. Ding, X. Wan, Y. B. Li, M. Jiang, C.-W. Qiu, S. Zhang, Electromagnetic reprogrammable codingmetasurface holograms, *Nat Commun.* 2017, 8: 197.